Butterfly distribution of relativistic electrons driven by parallel propagating lower band whistler chorus waves

Shinji Saito[1] and Yoshizumi Miyoshi[2]

[1]National Institute of Information and Communications Technology
[2]Institute for Space-Earth Environmental Research, Nagoya University

November 24, 2022

Abstract

We report results from a test particle simulation to reveal that electron scattering driven by lower band whistler chorus waves propagating along a magnetic field line plays an important role to produce the butterfly distribution of relativistic electrons. The results show that two nonlinear scattering processes, which are the phase trapping and the dislocation process, contribute to the formation of the butterfly distribution within a minute. We confirm that the quasilinear diffusion estimated from the whistler chorus waves are too slow to reproduce the butterfly distribution within a minute. The simulation results also show that there is the upper limit of rapid electron acceleration. We expect that the upper limit of the rapid flux enhancement is an evidence that the phase trapping process contributes to relativistic electron acceleration in the heart of the outer radiation belt.

Butterfly distribution of relativistic electrons driven by parallel propagating lower band whistler chorus waves

S. Saito[1,2] and Y. Miyoshi[2]

[1]Space environment Laboratory, Radio Propagation Research Center, Radio Research Institute, National Institute of Information and Communications Technology, Tokyo, Japan

[2]Institute for Space-Earth Environmental Research, Nagoya University, Nagoya, Japan

Key Points:

- A test particle simulation of electron scattering induced by lower band whistler chorus waves along a magnetic field line is carried out.
- The electron scattering with nonlinear properties produces butterfly distribution of relativistic electrons within a minute.
- The upper limit of electron acceleration for the butterfly distribution appears due to the upper limit of the nonlinear scattering.

Corresponding author: Shinji Saito, `s.saito@nict.go.jp`

Abstract

We report results from a test particle simulation to reveal that electron scattering driven by lower band whistler chorus waves propagating along a magnetic field line plays an important role to produce the butterfly distribution of relativistic electrons. The results show that two nonlinear scattering processes, which are the phase trapping and the dislocation process, contribute to the formation of the butterfly distribution within a minute. We confirm that the quasilinear diffusion estimated from the whistler chorus waves are too slow to reproduce the butterfly distribution within a minute. The simulation results also show that there is the upper limit of rapid electron acceleration. We expect that the upper limit of the rapid flux enhancement is an evidence that the phase trapping process contributes to relativistic electron acceleration in the heart of the outer radiation belt.

Plain Language Summary

Radiation belt electrons have various pitch angle distributions in response to global/local processes arising in the magnetosphere. Butterfly pitch angle distribution is a characteristic feature of the electron pitch angle distribution, which has the maximum flux intensity at a pitch angle lower than 90 degrees. Wave-particle interactions have been proposed as a driver for the butterfly distribution in the heart of the radiation belt. However, it is in debate how the wave-particle interactions contribute to the formation of the butterfly distribution of multi-megaelectron (MeV) volt electrons that is "killer electrons". In this Letter, we report that lower band whistler chorus waves play an important role for the electron butterfly distribution at MeV energies. A numerical simulation was carried out and showed that electrons nonlinearly scattered by the whistler chorus waves produce the butterfly distribution at MeV energies. The simulation also showed the upper limit of the rapid electron acceleration in the formation of the butterfly distribution. The simulation results advance our understanding of a formation mechanism of MeV electron butterfly distribution driven by whistler chorus waves.

1 Introduction

Dynamics in earth's magnetosphere causes variety of electron pitch angle distribution. One of characteristic features of electron pitch angle distribution in the magnetosphere is the butterfly distribution, which has the flux minimum at a pitch angle lower than 90°. A well-known cause of the butterfly distribution is the drift shell splitting (Roederer, 1967; Pfitzer et al., 1969; Sibeck et al., 1987; Selesnick & Blake, 2002). The day-night asymmetric magnetosphere is responsible for the butterfly distribution. Here, the drift shell is a closed surface on which trapped electrons travel around the Earth, and it expands more outward in the local noon in the case that electrons have higher equatorial pitch angles. In the case that the drift shell is in contact with the magnetopause boundary, electrons in the drift shell may escape into the interplanetary space, which is known as the magnetopause shadowing (MPS) process (Wilken et al., 1986; Matsumura et al., 2011). Following that leaking process of the electrons from the magnetosphere, the MPS contributes to the butterfly formation (West Jr. et al., 1973) by reducing the electron flux at high equatorial pitch angles. As another cause of the butterfly formation, it is proposed that electrons with high pitch angles are scattered due to large magnetic field curvature (Artemyev et al., 2015). The drift shell splitting, MPS, and the field curvature scattering are responsible for the butterfly distribution only in the outer edge of the outer radiation belt. However, Van Allen Probes observations have found butterfly distributions of relativistic electrons well inside the outer radiation belt (Ni et al., 2016). It suggests the butterfly distributions driven by some other physical mechanisms.

One of the mechanisms is quasilinear scattering process by wave-particle interactions. Xiao et al. (2015); Li et al. (2016) proposed a quasilinear diffusion process by magnetosonic (MS) waves with wavenumber almost perpendicular to magnetic field lines. The MS waves accelerate electrons at pitch angle of about 90° along the direction parallel to the magnetic field line by Landau resonant interactions. The scattering reduces the electron flux at about 90° pitch angle and increases the flux lower than 90° pitch angle, which results in the formation of the butterfly distribution. Another driver for the electron scattering is whistler chorus waves, which are intense, coherent, and right handed polarized electromagnetic waves naturally generated outside the plasmapause near the magnetic equator (LeDocq et al., 1998; Lauben et al., 2002; Parrot et al., 2003; Santolík et al., 2003; Miyoshi et al., 2003, 2013). In the case that energetic electrons are scattered at high magnetic latitudes, the whistler chorus waves could be responsible for the formation of the butterfly distribution (Horne & Thorne, 2003). On the other hand, the quasilinear diffusion model suggests that its contribution to the formation of butterfly distribution is low, and rather, the parallel propagating whistler chorus waves prevent the butterfly formation of relativistic electrons (Yang et al., 2016). Note that the quasilinear model does not include nonlinear scattering processes by intense whistler chorus waves. Test particle simulations (Gan et al., 2020; Saito et al., 2021) demonstrated that the nonlinear phase trapping by upper band whistler chorus waves causes pitch angle distributions of tens keV electrons to be butterfly shape in half a minute as observed by Van Allen Probes (Fennell et al., 2014) and Arase (Kurita et al., 2018). It suggests that the nonlinear scattering processes can be responsible for the formation of the butterfly distribution of radiation belt electrons. The test particle simulations demonstrated the contribution of the nonlinear scattering of the upper band whistler chorus waves to the butterfly distribution of tens keV electrons, but its contribution of the lower band whistler chorus (LBC) waves to MeV electrons has not been verified.

In order to investigate a formation process of the butterfly PAD of relativistic electrons, we have conducted a test particle simulation for the relativistic electron scattering by LBC waves propagating along a magnetic field line in the heart of the outer radiation belt. The simulation results showed that the LBC waves produce the butterfly distribution of relativistic electrons. We found that electrons satisfying the nonlinear scattering condition dominantly is responsible for the formation of the butterfly distribution of relativistic electrons. We evaluated that quasilinear diffusion coefficients derived from the LBC waves are insufficient for the flux enhancement in relativistic energies. Therefore, we conclude that the nonlinear scattering processes of LBC is important for the butterfly formation of relativistic electrons. The butterfly distribution could have a key information to identify whether the nonlinear scatterings contribute to the relativistic electron acceleration in the heart of the outer radiation belt.

2 Simulation model and parameters

The test particle simulation model used in this study is GEMSIS-RBW model Saito et al. (2012). The model solves the guiding center equation of motion for the adiabatic motion along a magnetic field line and the equation of motion for the nonadiabatic momentum change in time by whistler waves. The whistler waves propagate along the magnetic field line, satisfying the dispersion relation of the cold plasma. The details are described in Saito et al. (2012, 2016). The application to pulsating aurora and microbursts are found in Miyoshi et al. (2015, 2020, 2021).

The GEMSIS-RBW simulation demonstrates adiabatic and nonadiabatic motion of 10^6 electrons along the dipole magnetic field line at $L = 4$. The electrons are supposed to be lost at 100 km altitude, which corresponds to the equatorial loss cone angle of 5.47°. As the initial condition, test particles as electrons are uniformly distributed in the logarithm of energy E raging from 10 keV to 10 MeV and the equatorial pitch angle α_{eq} ranging from the loss cone to 90°. The random bounce and gyrophase are also given to each electron.

A particle weight is given to each electron using the particle weight method (Saito et al., 2021). The weights are given to reproduce the initial electron flux distribution corresponding to

$$j(E, \alpha_{eq}, t = 0) = j_0 \left(\frac{E}{E_0}\right)^{-p} \sin \alpha_{eq}, \tag{1}$$

where $j_0 = 10^4/\mathrm{cm}^2/\mathrm{str/keV/s}$ and $E_0 = 100$ keV. The index p is set as 2 and 4 at energies less and greater than E_0, respectively.

At $L = 4$, the electron gyrofrequency on the equatorial plane $f_{ce,eq}$ is 13.6 kHz. An ambient density of electron-proton pairs is supposed to be $N = 36.3$ cm^{-3} along the magnetic field line, which gives the electron plasma frequency f_{pe} of 54.0 kHz, so the frequency ratio $f_{pe}/f_{ce,eq}$ is given as 3.96 at the equator. Note that the ambient plasma density is set to be constant, so the frequency ratio becomes smaller at higher latitudes where the magnetic field becomes stronger. The dispersion relation of whistler waves applied in the test particle simulation depends on the ambient plasma condition along the magnetic field line.

The whistler waves in the simulation propagate parallel to the magnetic field line. We consider a lower band whistler chorus element with duration of 1 s and the frequency sweep rate $0.2f_{ce,eq}$ Hz/s at the equator. Each element is generated every 1 s, and propagates away from the equator up to the latitude of 50 degrees in both the northern and southern hemisphere. Each chorus element is coherent in this simulation model. Here the coherent means that the wave phase ϕ_w in the chorus element at the equator is continuous in time, which is described as $\phi_w = 2\pi f(t-t_0)$, where t is time, t_0 is the start time of the wave generation, and f is the frequency of the whistler chorus element which increases from $0.2f_{ce,eq}$ to $0.4f_{ce,eq}$ in 1 s. The magnetic wave amplitude δB_w is 300 pT, which is a kind of intense whistler chorus waves (e.g. Santolík et al., 2014). In this simulation, we calculated the electron scattering including nonlinear processes by cyclotron resonant interactions with the lower band whistler chorus elements propagating along the magnetic field line.

3 Results

Figure 1 shows the simulation results of electron flux distributions at the magnetic equator. Two panels in the left column are the flux distributions at (Upper panel) t=0 and (Lower panel) t = 60 s. The initial flux distribution corresponds to the flux distribution defined in Equation (1). The flux distribution at 60 s has a little change below 400 keV, but a significant increase of the flux is found at higher energies especially in the pitch angle ranging from 50° to 80°. The right panel shows the temporal variation of equatorial pitch angle distributions at four energy channels. The most efficient flux enhancement appears at energy of 2 MeV in the pitch angle ranging from 50° to 80°. In this pitch angle range, the flux at 2 MeV is about 20 times higher than the initial one, while the flux at 3.9 MeV is only about 2 times higher. It indicates that the energy spectrum becomes harder than the initial energy spectrum between 500 keV and 2 MeV, while the energy spectrum becomes softer between 2 MeV and 3.9 MeV. At pitch angles higher than 80°, the flux at energies less than 4 MeV decreases in 60 s.

Linear and nonlinear cyclotron resonant scatterings by whistler chorus waves depend on the energy and pitch angle of resonant electrons. Bortnik et al. (2008) classified the scattering process into three types by the parameter ρ. In the case of $\rho < 1$, the scattering becomes diffusive, which can be approximated by quasilinear diffusion process. In the case of $1 < \rho < 5$, the scattering satisfies a necessary condition for the nonlinear phase trapping which efficiently increases energy and pitch angle of electrons by the coherent whistler wave . In the case of $\rho > 5$, the scattering is the "dislocation" process which reduces the electron energy and the pitch angle. Except for the case of $\rho < 1$, the electron scattering is nonlinear, which cannot be described by conventional quasilinear diffusion models. After Bortnik et al. (2008) that defined ρ for nonrelativistic electrons, Saito et al. (2016) defined ρ_γ for relativistic electrons. The GEMSIS-RBW simulations (Saito et al., 2016, 2021) have confirmed that the parameter of ρ_γ can classify the scattering of relativistic electrons into the three types. Figure 2 shows the distribution of ρ_γ at three frequencies of whistler wave with the amplitude of 300 pT as a function of the pitch angle and energy. Here, the ρ_γ is calculated at magnetic latitudes where the first-order cyclotron resonant condition is satisfied along the magnetic field line. The solid and dashed lines show $\rho_\gamma = 1$ and $\rho_\gamma = 5$, respectively. Based on Bortnik et al. (2008), the region with $\rho_\gamma < 1$, $1 < \rho_\gamma < 5$, and $\rho_\gamma > 5$ are classified into the diffusion, the phase trapping, and the dislocation region, respectively. As an overall trend, the ρ_γ monotonically increases as the pitch angle increases. Thus, the region with pitch angle lower than the solid line's is the quasilinear diffusion region, the region with pitch angle higher than the dashed line's is the dislocation region, and the region between the solid and dashed lines is the phase trapping region.

The left panel of Figure 3 shows the increase rate of the electron flux in 60 s as a function of the equatorial pitch angle and energy. The solid and dashed line represent the $\rho_\gamma = 1$ and 5 contours with $f = 0.3 f_{ce,eq}$, respectively. Note that the shape of the phase trapping region is similar to that with $f = 0.2 f_{ce,eq}$ and $f = 0.4 f_{ce,eq}$ as shown in Figure 2. The increase rate indicates that the electron flux increases within the flux distribution ranges from 1 MeV to 3 MeV in energy and ranges from 50° to 80° in pitch angle. The maximum of the rate appears around the $\rho_\gamma = 1$ line, suggesting the contribution of the phase trapping process. On the other hand, the right side of the $\rho_\gamma =$ 5 line shows the flux decrease, indicating the contribution of the dislocation process. The right panel of Figure 3 shows the initial electron flux distribution of electrons responsible for the flux enhancement of the butterfly distribution in the green square at 60 s, where the green square ranges from 1.5 MeV to 3 MeV in energy and ranges from 56° to 70° in equatorial pitch angle. Here, to clarify the origin of electrons coming from outside the region of the enhanced butterfly distribution, electrons initially distributed in the green square are excluded in plotting the right panel. The lower limit of the initial distribution in energy is about 400 keV and that in pitch angle is about 20°. It indicates that a part of electrons gains energy over 1.1 MeV and its pitch angle changes over 36°. The integral omnidirectional electron flux of 2837.92 $[/\mathrm{cm}^2/\mathrm{s}]$ is transported into the green square from outside. Here, the amount of the flux is integrated in the distribution shown in the right panel of Figure 3. The flux transported from the diffusion region ($\rho_\gamma <$ 1), from the phase trapping ($1 < \rho_\gamma < 5$), and from the dislocation region ($\rho_\gamma > 5$) are 712.13 $[/\mathrm{cm}^2/\mathrm{s}]$ (25.1%), 2016.59 $[/\mathrm{cm}^2/\mathrm{s}]$ (71.1%), and 109.19 $[/\mathrm{cm}^2/\mathrm{s}]$ (3.8%), respectively. The electrons transported from the phase trapping region are dominant in the flux enhancement of the butterfly distribution at relativistic energies. The electrons initially distributed in the quasilinear diffusion region also contribute to the flux enhancement. We discuss the role of pitch angle diffusion process for the flux enhancement in the discussion and summary section. The electrons in the dislocation region have little impact on the flux enhancement, whereas it can be responsible for the formation of the butterfly distribution at relativistic energies by reducing the flux at the pitch angle of 90°.

Figure 4 shows bounce averaged diffusion coefficients of $\langle D_{EE}\rangle$ and $\langle D_{\alpha_{eq}\alpha_{eq}}\rangle$ by the parallel propagating whistler waves with the wave amplitude of 300 pT and with the frequencies between $0.2f_{ce,eq}$ and $0.4f_{ce,eq}$. The diffusion coefficients are calculated according to Shprits et al. (2006). The black solid and dashed line represent the $\rho_\gamma = 1$ and 5 contour lines with $f = 0.3f_{ce,eq}$, respectively. The top panels show the diffusion coefficients at the cyclotron resonance with $k_\parallel v_\parallel > 0$ and the middle panels show those with $k_\parallel v_\parallel < 0$, where $v_\parallel$ is the resonant electron velocity and $k_\parallel$ is the wavenumber of the whistler wave. Note that the cyclotron resonance condition with $k_\parallel v_\parallel > 0$ can be satisfied in relativistic energies. The boundary between the two resonance conditions crosses the line of $\rho_\gamma = 1$. The crossing area is in the green square same as in Figure 3 where the electron flux has the maximum increase rate. Lower panels in Figure 4 show the electron diffusion coefficients at 512.5 keV as a function of the pitch angle. In the quasilinear diffusion region ($\alpha_{eq} < 60°$ at 512.5 keV), the diffusion coefficients $\langle D_{EE}\rangle/E^2$ and $\langle D_{\alpha_{eq}\alpha_{eq}}\rangle$ are less than 5×10^{-4} and 10^{-3}, respectively. The diffusion coefficients are considered as

$$\langle D_{\alpha_{eq}\alpha_{eq}}\rangle = \frac{\Delta\alpha_{eq}^2}{2\Delta t}, \tag{2}$$

$$\frac{\langle D_{EE}\rangle}{E^2} = \frac{\Delta E^2}{2\Delta t E^2}, \tag{3}$$

where ΔE and $\Delta\alpha_{eq}$ are variation in energy and equatorial pitch angle during the time of Δt. As electrons have $\langle D_{EE}\rangle/E^2 = 5\times10^{-4}$ and $\langle D_{\alpha_{eq}\alpha_{eq}}\rangle = 10^{-3}$, the variations can be estimated as $\Delta E = 125$keV and $\Delta\alpha_{eq} = 19.8°$ with $\Delta t = 60$ s, respectively. Considering that electrons with the initial energy of 512.5 keV and with the equatorial pitch angle of 40° ($\rho_\gamma = 1$), these electrons are necessary to have the energy gain $\Delta E =$ 987.5–2487.5 keV and the equatorial pitch angle change $\Delta\alpha_{eq} = 16$–$30°$ to produce the butterfly formation that appears in the green square shown in Figure 3. Here, the green square ranges from 1.5 MeV to 3 MeV in energy and 56° to 70° in equatorial pitch angle. The variation in equatorial pitch angle obtained from the GEMSIS-RBW simulation is comparable to that estimated from the quasilinear model ($\Delta\alpha_{eq} = 19.8°$). However, the energy gain estimated from the quasilinear model ($\Delta E = 125$keV) is insufficient to contribute to the butterfly formation, which indicates that quasilinear diffusion is too slow to produce the butterfly distribution in the short time.

4 Discussion and summary

It has been argued that magnetosonic (MS) waves with wavenumber almost perpendicular to magnetic field lines play an important role for the formation of the butterfly pitch angle distribution of relativistic electrons (Xiao et al., 2015; Li et al., 2016). On the other hand, whistler chorus waves are considered to suppress the formation of the butterfly distribution (Yang et al., 2016). However, our simulation results showed that lower band whistler chorus waves (LBC) propagating parallel to the magnetic field line produce the butterfly distribution of relativistic electrons (Figure 1) by the contribution of the phase trapping and the dislocation process (Figure 2 and 3). Our simulation results also showed that the quasilinear diffusion process is insufficient to produce relativistic electrons responsible for the formation of the butterfly distribution within a minute (Figure 4). We conclude that nonlinear scattering processes (the phase trapping and the dislocation) by LBC play a key role to rapidly produce the butterfly distribution of relativistic electrons.

The maximum of the flux increase rate appears in energy of about 2 MeV and in pitch angle of about 60° (Figure 3). The flux increase rate becomes lower at energies higher than 2 MeV (Figure 3), and the butterfly formation is less pronounced (Figure 1). It indicates that the efficient transport of electrons from lower energies is terminated. The terminal region is located in the crossing area between the $\rho_\gamma = 1$ line and the boundary where sign of $k_\parallel v_\parallel$ is inverted (Figure 4). In the case of the cyclotron resonance with $k_\parallel v_\parallel < 0$, the equatorial pitch angle of the resonant electron increases with increasing the energy according to diffusion curves (e.g. Summers et al., 1998). The phase trapping also show the same trend, as in the case of the Relativistic Turning Acceleration (RTA) before the turning process (Omura et al., 2008). The phase trapping region shifts to higher pitch angles at higher energies, so that the electron tends to remain within the phase trapping region during acceleration. However, in the case of the cyclotron resonance with $k_\parallel v_\parallel > 0$ at relativistic energies, the pitch angle decreases with increasing the energy (e.g. Summers et al., 1998). The phase trapping at relativistic energies also decreases the pitch angle while increasing the energy, as in the case of the Ultra Relativistic Acceleration (URA) process (Summers & Omura, 2007) and the RTA after the turning process (Omura et al., 2008). Thus, the relativistic electron in the phase trapping region move into the quasilinear diffusion region ($\rho_\gamma < 1$) by reducing its pitch angle. Therefore, the efficient acceleration through the phase trapping is terminated due to changes of ρ_γ, that makes the upper limit in energy and the peak position in pitch angle of the butterfly distribution. We expect that the presence of the upper limit of the flux enhancement in energy is a nonlinear signature of the electron acceleration. Ni et al. (2016) showed that relativistic electron butterfly distributions are likely to peak between 58° and 79° in pitch angle on $L = 4$ from the Van Allen Probes observations. Our simulation result is consistent with the observation. We need more case studies to examine whether the formation of the butterfly distribution of relativistic electrons seen in the observations is controlled by the crossing area between the $\rho_\gamma = 1$ line and the boundary where the sign of $k_\parallel v_\parallel$ is inverted.

The simulation results show that electrons initially distributed in the diffusion region ($\rho_\gamma < 1$) are also responsible for the flux enhancement of the butterfly distribution (Figure 3). The plausible scenario is that these electrons are scattered into the phase trapping region through the quasilinear diffusion in pitch angle, and then efficiently accelerated through the phase trapping. We have confirmed that diffusion curves of the electrons are along the pitch angle direction with the almost constant energy in this case (Summers et al., 1998). Also, the quasilinear pitch angle diffusion coefficients indicate that the electrons can change the pitch angle by about 20° in 60 s (Figure 4). Therefore, the electrons located about 20° away from the pitch angle of $\rho_\gamma = 1$ line can come into the phase trapping region, and then contribute to the formation of the butterfly distribution in relativistic energies. We conclude that the quasilinear diffusion process has an important role in the preconditioning to supply electrons into the phase trapping region from low pitch angles.

Electrons with energies less than about 400 keV are not efficiently accelerated into relativistic energies even within the phase trapping region (Figure 3). The simulation result suggests that the efficient acceleration by the phase trapping requires additional conditions depend on electron energy. Detail studies for the acceleration process of lower energy electrons is necessary as a future work.

The initial flux distribution at relativistic energies is supposed to have the power law index of -4 in the simulation shown here, whose gradient in energy is relatively steep.

The butterfly formation could be more prominent at relativistic energies in the case of steeper flux gradients in energy, because more electron flux can be supplied to the relativistic energies. Thus, the electron distribution with harder energy spectrum may produce more relaxed butterfly distributions than that shown in the simulation. The dependence of the initial energy spectrum on the formation of the butterfly distribution is also required as a future work.

Acknowledgments

This work was supported by JSPS KAKENHI Grant Number JP20H01959. The test particle data obtained from the RBW simulation and the software (python scripts) used to produce figures in the Letter are publicly available online (https://doi.org/10.5281/zenodo.6430412).

References

Artemyev, A. V., Agapitov, O. V., Mozer, F. S., & Spence, H. (2015). Butterfly pitch angle distribution of relativistic electrons in the outer radiation belt: Evidence of nonadiabatic scattering. *Journal of Geophysical Research: Space Physics*, *120*(6), 4279–4297. doi: 10.1002/2014ja020865

Bortnik, J., Thorne, R. M., & Inan, U. S. (2008). Nonlinear interaction of energetic electrons with large amplitude chorus. *Geophysical Research Letters*, *35*(L21102). doi: https://doi.org/10.1029/2008GL035500

Fennell, J. F., Roeder, J. L., Kurth, W. S., Henderson, M. G., Larsen, B. A., Hospodarsky, G., . . . Reeves, G. D. (2014). Van Allen Probes observations of direct wave-particle interactions. *Geophysical Research Letters*, *41*(6), 1869-1875. doi: https://doi.org/10.1002/2013GL059165

Gan, L., Li, W., Ma, Q., Artemyev, A. V., & Albert, J. M. (2020). Unraveling the formation mechanism for the bursts of electron butterfly distributions: Test particle and quasilinear simulations. *Geophysical Research Letters*, *47*(21), e2020GL090749. doi: https://doi.org/10.1029/2020GL090749

Horne, R. B., & Thorne, R. M. (2003). Relativistic electron acceleration and precipitation during resonant interactions with whistler-mode chorus. *Geophysical Research Letters*, *30*(10). doi: https://doi.org/10.1029/2003GL016973

Kurita, S., Miyoshi, Y., Kasahara, S., Yokota, S., Kasahara, Y., Matsuda, S., . . . Shinohara, I. (2018). Deformation of electron pitch angle distributions caused by upper band chorus observed by the Arase satellite. *Geophysical Research Letters*, *45*(16), 7996-8004. doi: https://doi.org/10.1029/2018GL079104

Lauben, D. S., Inan, U. S., Bell, T. F., & Gurnett, D. A. (2002). Source characteristics of ELF/VLF chorus. *Journal of Geophysical Research: Space Physics*, *107*(A12), SMP 10-1-SMP 10-17. doi: https://doi.org/10.1029/2000JA003019

LeDocq, M. J., Gurnett, D. A., & Hospodarsky, G. B. (1998). Chorus source locations from VLF poynting flux measurements with the Polar spacecraft. *Geophysical Research Letters*, *25*(21), 4063-4066. doi: https://doi.org/10.1029/1998GL900071

Li, J., Bortnik, J., Thorne, R. M., Li, W., Ma, Q., Baker, D. N., ... Blake, J. B. (2016). Ultrarelativistic electron butterfly distributions created by parallel acceleration due to magnetosonic waves. *Journal of Geophysical Research: Space Physics*, *121*(4), 3212-3222. doi: https://doi.org/10.1002/2016JA022370

Matsumura, C., Miyoshi, Y., Seki, K., Saito, S., Angelopoulos, V., & Koller, J. (2011). Outer radiation belt boundary location relative to the magnetopause: Implications for magnetopause shadowing. *Journal of Geophysical Research: Space Physics (19782012)*, *116*(A6). doi: 10.1029/2011ja016575

Miyoshi, Y., Hosokawa, K., Kurita, S., Oyama, S.-I., Ogawa, Y., Saito, S., ... Nakamura, S. (2021). Penetration of MeV electrons into the mesosphere accompanying pulsating aurorae. *Scientific Reports*, *11*(13724). doi: 10.1038/s41598-021-92611-3

Miyoshi, Y., Kataoka, R., Kasahara, Y., Kumamoto, A., Nagai, T., & Thomsen, M. F. (2013). High-speed solar wind with southward interplanetary magnetic field causes relativistic electron flux enhancement of the outer radiation belt via enhanced condition of whistler waves. *Geophysical Research Letters*, *40*(17), 4520-4525. doi: https://doi.org/10.1002/grl.50916

Miyoshi, Y., Morioka, A., Misawa, H., Obara, T., Nagai, T., & Kasahara, Y. (2003). Rebuilding process of the outer radiation belt during the 3 november 1993 magnetic storm: NOAA and Exos-D observations. *Journal of Geophysical Research: Space Physics*, *108*(A1), SMP 3-1-SMP 3-15. doi: https://doi.org/10.1029/2001JA007542

Miyoshi, Y., Saito, S., Kurita, S., Asamura, K., Hosokawa, K., Sakanoi, T., ... Blake, J. B. (2020). Relativistic electron microbursts as high-energy tail of pulsating aurora electrons. *Geophysical Research Letters*, *47*(21), e2020GL090360. doi: https://doi.org/10.1029/2020GL090360

Miyoshi, Y., Saito, S., Seki, K., Nishiyama, T., Kataoka, R., Asamura, K., ... Santolik, O. (2015). Relation between fine structure of energy spectra for pulsating aurora electrons and frequency spectra of whistler mode chorus waves. *Journal of Geophysical Research: Space Physics*, *120*(9), 7728-7736. doi: https://doi.org/10.1002/2015JA021562

Ni, B., Zou, Z., Li, X., Bortnik, J., Xie, L., & Gu, X. (2016). Occurrence characteristics of outer zone relativistic electron butterfly distribution: A survey of van allen probes REPT measurements. *Geophysical Research Letters*, *43*(11), 5644-5652. doi: https://doi.org/10.1002/2016GL069350

Omura, Y., Katoh, Y., & Summers, D. (2008). Theory and simulation of the generation of whistler-mode chorus. *Journal of Geophysical Research: Space Physics*, *113*(A4). doi: https://doi.org/10.1029/2007JA012622

Parrot, M., Santolík, O., Cornilleau-Wehrlin, N., Maksimovic, M., & Harvey, C. C. (2003). Source location of chorus emissions observed by cluster. *Annales Geophysicae*, *21*(2), 473–480. Retrieved from `https://angeo.copernicus.org/articles/21/473/2003/` doi: 10.5194/angeo-21-473-2003

Pfitzer, K. A., Lezniak, T. W., & Winckler, J. R. (1969). Experimental verification of drift-shell splitting in the distorted magnetosphere. *Journal of Geophysical Research (1896-1977)*, *74*(19), 4687-4693. Retrieved from `https://agupubs.onlinelibrary.wiley.com/doi/abs/10.1029/JA074i019p04687` doi: https://doi.org/10.1029/JA074i019p04687

Roederer, J. G. (1967). On the adiabatic motion of energetic particles in a model magnetosphere. *Journal of Geophysical Research*, *72*(3), 981–992. doi: 10.1029/jz072i003p00981

Saito, S., Kurita, S., Miyoshi, Y., Kasahara, S., Yokota, S., Keika, K., ... Shinohara, I. (2021). Data-driven simulation of rapid flux enhancement of energetic electrons with an upper-band whistler burst. *Journal of Geophysical Research: Space Physics*, *126*(4), e2020JA028979. doi: https://doi.org/10.1029/2020JA028979

Saito, S., Miyoshi, Y., & Seki, K. (2012). Relativistic electron microbursts associated with whistler chorus rising tone elements: GEMSIS-RBW simulations. *Jour-*

nal of Geophysical Research: Space Physics, *117*(A10). doi: https://doi.org/10.1029/2012JA018020

Saito, S., Miyoshi, Y., & Seki, K. (2016). Rapid increase in relativistic electron flux controlled by nonlinear phase trapping of whistler chorus elements. *Journal of Geophysical Research: Space Physics*, *121*(7), 6573-6589. doi: https://doi.org/10.1002/2016JA022696

Santolík, O., Gurnett, D. A., Pickett, J. S., Parrot, M., & Cornilleau-Wehrlin, N. (2003). Spatio-temporal structure of storm-time chorus. *Journal of Geophysical Research: Space Physics*, *108*(A7). doi: https://doi.org/10.1029/2002JA009791

Santolík, O., Kletzing, C. A., Kurth, W. S., Hospodarsky, G. B., & Bounds, S. R. (2014). Fine structure of large-amplitude chorus wave packets. *Geophysical Research Letters*, *41*(2), 293-299. doi: https://doi.org/10.1002/2013GL058889

Selesnick, R. S., & Blake, J. B. (2002). Relativistic electron drift shell splitting. *Journal of Geophysical Research: Space Physics*, *107*(A9), SMP 27-1-SMP 27-10. doi: https://doi.org/10.1029/2001JA009179

Shprits, Y. Y., Thorne, R. M., Horne, R. B., & Summers, D. (2006). Bounce-averaged diffusion coefficients for field-aligned chorus waves. *Journal of Geophysical Research: Space Physics*, *111*(A10). doi: https://doi.org/10.1029/2006JA011725

Sibeck, D. G., McEntire, R. W., Lui, A. T. Y., Lopez, R. E., & Krimigis, S. M. (1987). Magnetic field drift shell splitting: Cause of unusual dayside particle pitch angle distributions during storms and substorms. *Journal of Geophysical Research: Space Physics (19782012)*, *92*(A12), 13485–13497. doi: 10.1029/ja092ia12p13485

Summers, D., & Omura, Y. (2007). Ultra-relativistic acceleration of electrons in planetary magnetospheres. *Geophysical Research Letters*, *34*(24). doi: https://doi.org/10.1029/2007GL032226

Summers, D., Thorne, R. M., & Xiao, F. (1998). Relativistic theory of wave-particle resonant diffusion with application to electron acceleration in the magnetosphere. *Journal of Geophysical Research: Space Physics*, *103*(A9), 20487-20500. doi: https://doi.org/10.1029/98JA01740

West Jr., H. I., Buck, R. M., & Walton, J. R. (1973). Electron pitch angle distributions throughout the magnetosphere as observed on Ogo 5. *Journal of Geophysical Research (1896-1977)*, *78*(7), 1064-1081. doi: https://doi.org/10.1029/JA078i007p01064

Wilken, B., Baker, D., Higbie, P., Fritz, T., Olson, W., & Pfitzer, K. (1986). Magnetospheric configuration and energetic particle effects associated with a SSC: A case study of the CDAW 6 Event on March 22, 1979. *Journal of Geophysical Research: Space Physics*, *91*(A2), 1459. doi: 10.1029/ja091ia02p01459

Xiao, F., Yang, C., Su, Z., Zhou, Q., He, Z., He, Y., ... Blake, J. B. (2015). Wave-driven butterfly distribution of Van Allen belt relativistic electrons. *Nature Commun*, *6*(1), 8590. doi: https://doi.org/10.1038/ncomms9590

Yang, C., Su, Z., Xiao, F., Zheng, H., Wang, Y., Wang, S., ... Funsten, H. O. (2016). Rapid flattening of butterfly pitch angle distributions of radiation belt electrons by whistler-mode chorus. *Geophysical Research Letters*, *43*(16), 8339-8347. doi: https://doi.org/10.1002/2016GL070194

Figure captions

Figure 1

(The left panels) Equatorial electron flux distributions as a function of the equatorial pitch angle and the energy at t = 0 and 60 s. (The right panel) The electron pitch angle distributions at four energy channels (491.1 keV, 1. 1 MeV, 2 MeV, and 3.9 MeV) at t=0, 20, 40, and 60 s.

Figure 2

The distribution of ρ_γ as a function of the equatorial pitch angle and the energy with whistler wave frequency of $0.2 f_{ce,eq}$, $0.3 f_{ce,eq}$, and $0.4 f_{ce,eq}$. The solid and dashed lines correspond to contour lines of $\rho_\gamma = 1$ and 5, respectively.

Figure 3

(Left panel) The ratio of the electron fluxes at t=0 and t=60 s. (Right panel) The distribution of the origin of electrons scattered into the green square region ranging from 1.5 MeV to 3 MeV in energy and from 56° to 70° in equatorial pitch angle at t = 60 s.

The solid and dashed lines in both panels corresponds to the contour lines of $\rho_\gamma = 1$ and 5 with whistler wave frequency of $0.3 f_{ce,eq}$, respectively.

Figure 4

(The left panels) The bounce averaged diffusion coefficients in equatorial pitch angle. (The right panels) The bounce averaged diffusion coefficients in energy. (The top panels) The bounce averaged diffusion coefficients in the cyclotron resonance condition satisfying $k_\parallel v_\parallel > 0$. (The middle panels) The bounce averaged diffusion coefficients in the cyclotron resonance condition satisfying $k_\parallel v_\parallel < 0$. The solid and dashed lines correspond to the lines of $\rho_\gamma = 1$ and 5 with whistler wave frequency of $0.3 f_{ce,eq}$, respectively. (The bottom panels) The bounce averaged diffusion coefficients at energy of 512.5 keV.

Figure 1.

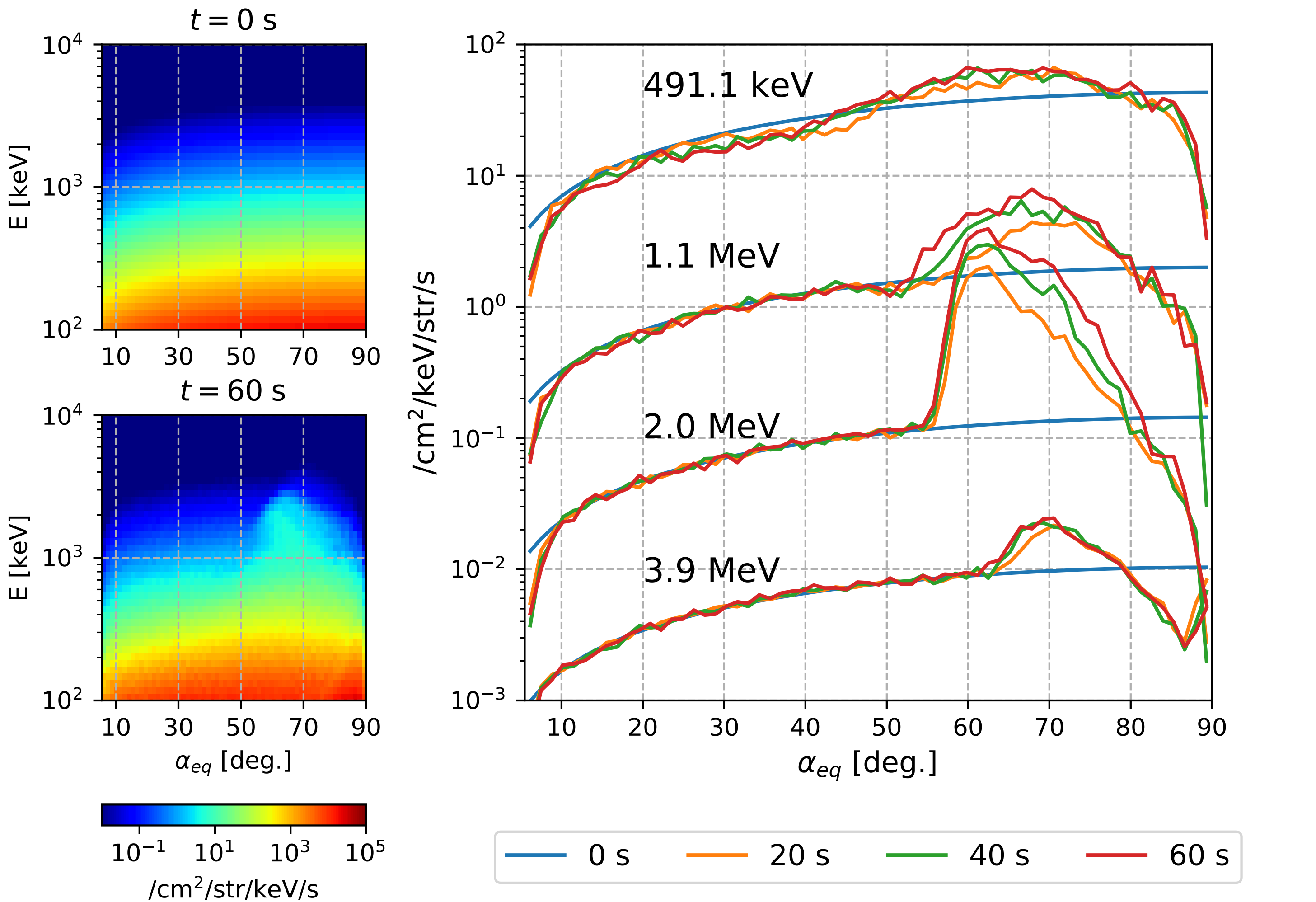

$t = 0$ s
$t = 60$ s
E [keV]
α_{eq} [deg.]
/cm^2/str/keV/s
491.1 keV
1.1 MeV
2.0 MeV
3.9 MeV
/cm^2/keV/str/s
0 s
20 s
40 s
60 s

Figure 2.

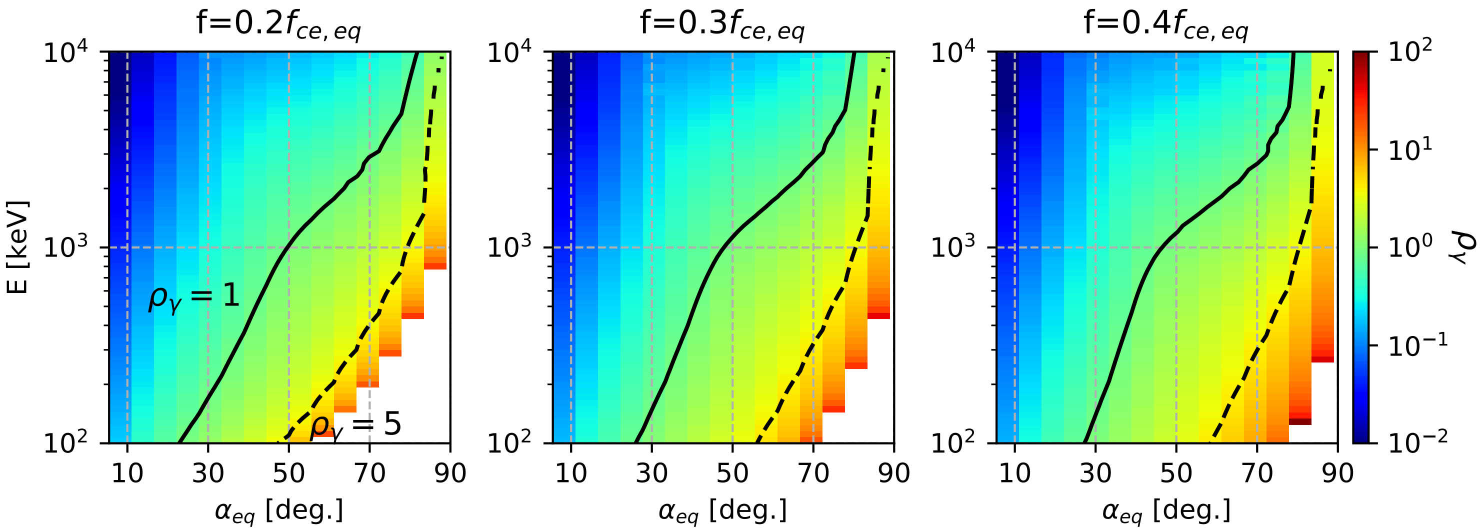

f=0.2$f_{ce,eq}$
f=0.3$f_{ce,eq}$
f=0.4$f_{ce,eq}$
E [keV]
10^4
10^3
10^2
$\rho_\gamma = 1$
$\rho_\gamma = 5$
10 30 50 70 90
α_{eq} [deg.]
ρ_γ
10^2
10^1
10^0
10^{-1}
10^{-2}

Figure 3.

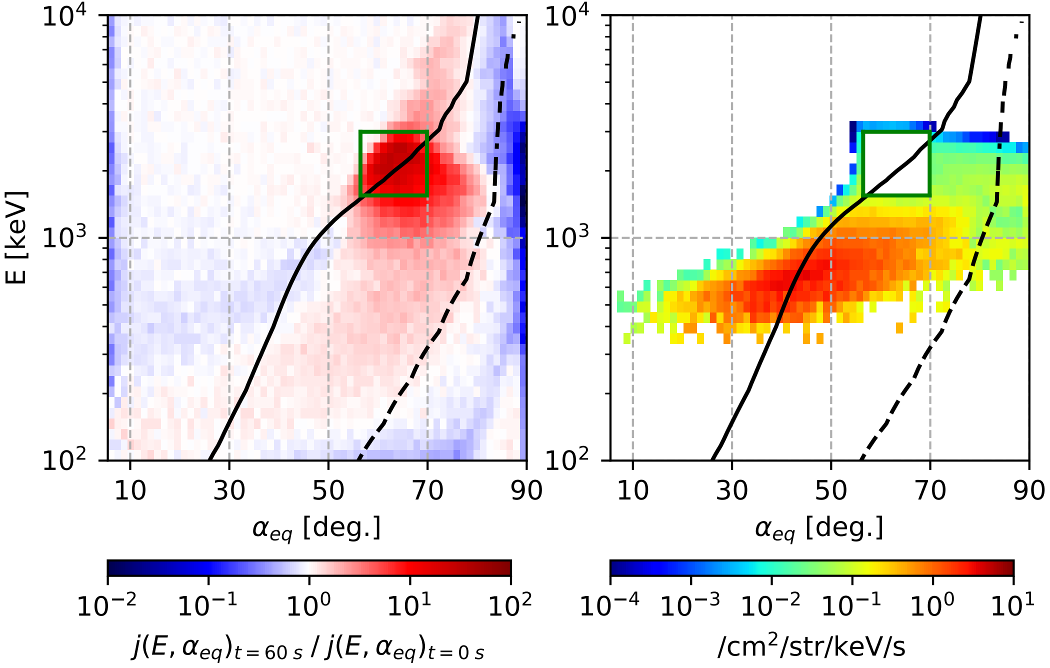

10^4
10^3
10^2
E [keV]
10
30
50
70
90
α_{eq} [deg.]
10^{-2}
10^{-1}
10^0
10^1
10^2
$j(E, \alpha_{eq})_{t=60\ s}$ / $j(E, \alpha_{eq})_{t=0\ s}$
10^4
10^3
10^2
10
30
50
70
90
α_{eq} [deg.]
10^{-4}
10^{-3}
10^{-2}
10^{-1}
10^0
10^1
/cm^2/str/keV/s

Figure 4.

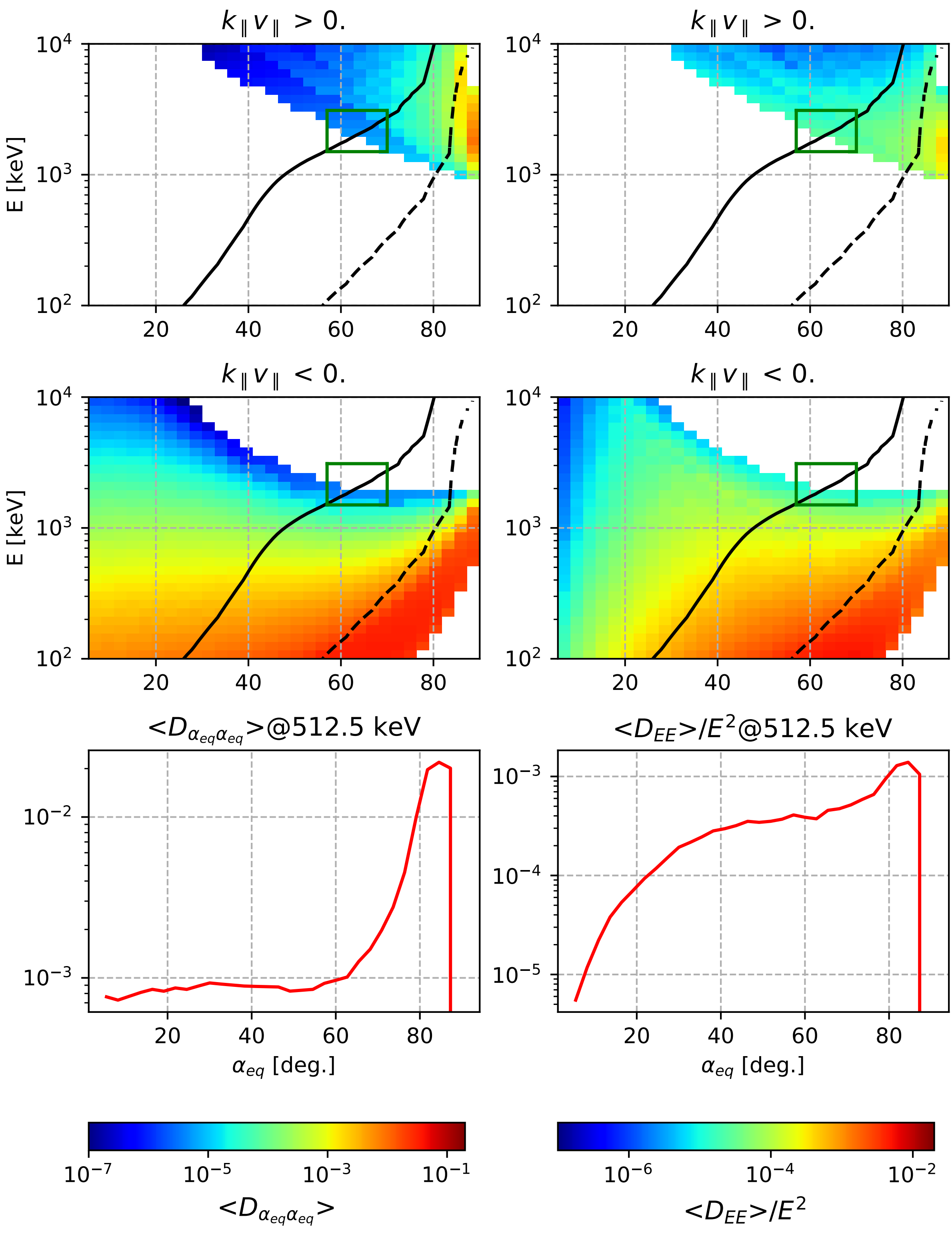

$k_\parallel v_\parallel > 0.$
$k_\parallel v_\parallel > 0.$
$k_\parallel v_\parallel < 0.$
$k_\parallel v_\parallel < 0.$
E [keV]
$<D_{\alpha_{eq}\alpha_{eq}}>$@512.5 keV
$<D_{EE}>/E^2$@512.5 keV
α_{eq} [deg.]
$<D_{\alpha_{eq}\alpha_{eq}}>$
$<D_{EE}>/E^2$